MACHINE VISION BASED MEASUREMENT OF DYNAMIC CONTACT ANGLES IN MICROCHANNEL FLOWS

Journal of Bionic Engineering Manuscript

Valtteri Heiskanen
Micro- and Nanosystems Research Group,
Department of Automation Science and Engineering

Kalle Marjanen
Measurements Based on Images Research Group,
Department of Automation Science and Engineering

Pasi Kallio
Micro- and Nanosystems Research Group,
Department of Automation Science and Engineering

P.O. Box 692
33101 Tampere
FINLAND
Tel: +358 50 052 5546
E-mail: pasi.kallio@tut.fi

ABSTRACT

When characterizing flows in miniaturized channels, the determination of the dynamic contact angle is important. By measuring the dynamic contact angle, the flow properties of the flowing liquid and the effect of material properties on the flow can be characterized. A machine vision based system to measure the contact angle of front or rear menisci of a moving liquid plug is described in this article. In this research, transparent flow channels fabricated on thermoplastic polymer and sealed with an adhesive tape are used. The transparency of the channels enables image based monitoring and measurement of flow variables, including the dynamic contact angle. It is shown that the dynamic angle can be measured from a liquid flow in a channel using the image based measurement system. An image processing algorithm has been developed in a MATLAB environment. Images are taken using a CCD camera and the channels are illuminated using a custom made ring light. Two fitting methods are experimented and the results compared in the measurement of the dynamic contact angles; a circle and two parabolas.

Keywords: *Digital Image Processing, Machine Vision, Microfluidics, Microchannel Flow, Dynamic Contact Angle, Image Based Measurement*

1 INTRODUCTION

The measurement of a contact angle (or a wetting angle) is used in the analysis of material surface properties. Based on the contact angle, the contact can be classified either as hydrophopic (contact angle > 90°) or hydrophilic (contact angle < 90°) [1]. The contact angles can be divided into static contact angles and dynamic contact angles. The measurement of the static contact angle is most commonly based on a droplet analysis. A small droplet of test liquid is placed on the surface of material to be analyzed. Image based methods are common when measuring the static contact angle [2-3]. Microscopy is used as well [4]. The dynamic contact angle is measured when liquid is moving on a material. Here, the contact angle can be measured from the front or rear meniscus of a moving liquid plug. It has been shown that the dynamic contact angle can significantly differ when comparing to the static contact angle [5]. The dependency of the dynamic contact angle on the velocity of a liquid plug and variations caused by surface properties are not very well known. Generally, as the velocity increases, the dynamic contact angle increases as well. Measuring the dynamic contact angle can be a challenging task; the Wilhelmy method using a dynamic contact angle meter is useful in some cases [6]. However, measuring the angle directly from a channel structure is difficult with this method. Transparency of channels enables image based

measurements of the dynamic contact angles as it will be shown in this article. Li, Kang and Ye suggested that a contact angle can be measured precisely by extracting a liquid droplet coordinates and fitting a circle to them [2]. This method modified for microchannel applications was found useful in this study.

Measuring the dynamic contact angle is important when studying the effect of the microchannel properties, such as channel dimensions and cross-sectional profiles, on the plug flow. The measurement of the dynamic contact angle becomes useful also when studying surface properties of micro- and nanochannel materials as well as in understanding the dynamics in air-liquid interfaces. Also, the effect of the liquid properties on the flow behavior is needed to be characterized. The capillary pressure drop in a channel can be modeled and determined based on the dynamic contact angle [1]. When designing and experimenting capillary burst valves, the possibility of determining the dynamic contact angle is a benefit, since the pressure difference across the burst valve is dependent on the dynamic contact angle [7-8]. In industrial production, quality control of microchips and biochips could be performed by analyzing the dynamic contact angles.

The objective of this study is to study machine vision based methods to measure dynamic contact angles in microchannel flows using digital images. The rest of the article is organized as follows. The measurement system and the channel structures used in the research are presented in Section 2. Section 3 describes the algorithm development performed in MATLAB software environment. Experimental measurement results using the algorithm developed are described in Section 4 and Section 5 provides a conclusion of this research.

2 MEASUREMENT SETUP

This section describes the measurement setup and the channels used in the study. The channel structures are described in Subsection 2.1 and Subsection 2.2 discusses the measurement system.

2.1 Flow Channel Structures:

Miniaturized channel structures fabricated on Methyl methacrylate-acrylonitrile butadiene styrene (MABS) and sealed with an adhesive tape are used in the experiments of this research. The structures are fabricated by mechanical milling and are specifically designed for experiments in characterizing flows in miniaturized channels. In adhesive bonding, a piece of an adhesive tape is installed on that side of the structure where the channels are machined. The adhesive tape used for sealing is Adhesive Research ARseal 90404 1-sided tape [9]. The static contact angle measured for the tape is approximately 90° with

De-ionised (DI) water. DI water is also used as a test liquid in the channel experiments. MABS is hydrophilic material (the measured static contact angle with DI water is approximately 67°) but the sealed channels are hydrophobic due to the adhesive tape. The channel structure consists of different channels; five wide channels incorporating passive valves and four small narrow channels. Two of the wide channels are used in this study. The first channel, CH1, is divided into two larger sections (Sections A and B) which are separated by a passive valve. Section A is used in the experiments, since it has one inlet connection. Section B has two connections designed for performing more complicated studies. Channel CH1 has a rectangular cross-section with a width of 2000 µm and a height of 300 µm. The second used channel, CH2, has three circular widening sections designed for other experiments. However, only the sections with a constant cross-sectional area of 1000 µm x 300 µm are used in this study. The channel dimensions given here are the design values, not measured. However, based on the image analysis, the deviation of the actual channel dimensions from the designed values is not significant. The workshop drawings of the channels are illustrated in Fig. 1. Half-filled Section A of Channel CH1 is depicted in Fig. 2.

2.2 Machine Vision based Measurement System:

Liquid is driven in the channels using a flow control device. In this study, a syringe pump (NE-501 Multi-Phaser of New Era Pump Systems Inc.) is used for the flow control. The syringe pump is connected to the channel inlet by using pipettes having a conic tip. The imaging of the channel structure can be performed using a digital camera when the resolution [1/mm] in a target plane is adequate and have modulation transfer functions (MTF) satisfactory to repeat detected frequencies. A digital Firewire camera (Sony XCD-X710) is used with Optem's Macro Video Zoom Lens (MVZL) for imaging the channel flows. A custom made ring light is used as an illumination source. As light sources, high current Luxeon Star LEDs are used. The ring light consists of eight red light LEDs and eight white light LEDs which are possible to use separately or simultaneously.

The images are transferred to a computer using a digital Firewire b-connection. The acquired images are then further processed to extract the desired quantities. MATLAB® software from Mathworks is used for the algorithm development. The acquired image data is processed off-line with the developed algorithm.

The measurement setup and a photograph of the system are illustrated in Fig. 3 and Fig. 4, respectively.

3 MEASUREMENT PRINCIPLE OF THE DYNAMIC CONTACT ANGLE

The determination of the dynamic contact angle from the digital image data is described in this section. The measurement algorithm is divided into two parts; image processing and computation methods of the contact angle, which are described in Subsections 3.1 (image processing), 3.2 (computation using circle fitting) and 3.3 (computation using parabola fitting) respectively.

The dynamic contact angle can be determined from the top and bottom contact points in a channel, as illustrated in Fig. 5. In this study, both the top and bottom dynamic contact angles, θ_t and $\theta_{b,}$ are determined separately.

Two methods have been considered for the computation of the dynamic contact angles. First, a circle fit to the liquid meniscus is studied. In high-velocity liquid flows however, the meniscus becomes non-circular. In such cases, the determination of the dynamic contact angle using the circle fitting becomes significantly inaccurate. Therefore, parabola fitting is also experimented.

3.1 Image Processing Methods:

The aim of the image processing part is to find the coordinates of the front and rear menisci. The meniscus detection is based on image series acquired from the flow channel. Two consecutive images are subtracted and the result is then thresholded [10]. The resulting binary image consists of zeros and ones. Image regions, having a value of one (so called blobs), represent the moved liquid plug between two images.

The threshold selection is important and it is selected such that the blob representing the liquid plug can be extracted properly. Here, the determination of the threshold is done using in-house developed software. In the software, the user can vary the threshold values in the beginning of the experiment and by observing the resulting binary image, determine a proper threshold value for the case.

After thresholding, the profile of the meniscus is extracted by searching its x- and y-coordinates. In the algorithm, the direction of the liquid flow is assumed to be horizontal. Based on the direction of the flow in the image series, the coordinates can be located by detecting every row in a single binary image separately. By locating the first pixel having value one in each row, the coordinates of the meniscus can be detected. The extraction of the front meniscus is illustrated in Fig. 6.

After the extraction of the meniscus coordinates, either a circle or a parabola fitting is applied. Once a proper fitting is found, the dynamic contact angles can be computed. In the following, computation of the

dynamic contact angle is presented for the front meniscus. The computation can be similarly performed for the rear meniscus.

3.2 Contact Angle Computation using Circle Fitting:

After the determination of the meniscus coordinates, the next steps are as follows: i) fitting a circle to the coordinates, ii) finding the contact points (x_t,y_t) and (x_b,y_b) at the top and bottom surfaces as illustrated in Fig. 7, iii) determining the contact angle using the circle equation and the contact points. The steps are described in more details in the following.

As the coordinates of the front meniscus are located, a proper circle fitting can be found by solving a circle equation. The basic equation of a circle can be written as follows

$$(x - x_0)^2 + (y - y_0)^2 = r^2 \tag{1}$$

where x and y are the meniscus profile coordinates, x_0 and y_0 are the circle center coordinates and r is the circle radius.

The equation can be rewritten as:

$$x^2 + y^2 + a_c x + b_c y + c_c = 0 \tag{2}$$

where:

$$a_c = -2x_0$$
$$b_c = -2y_0$$
$$c_c = x_0^2 + y_0^2 - r^2$$

The parameters a_c, b_c and c_c can be solved using the least squares method from the following equation

$$\begin{bmatrix} a_c \\ b_c \\ c_c \end{bmatrix} \begin{bmatrix} x & y & 1 \end{bmatrix} = -x^2 - y^2 \tag{3}$$

The contact points (x_t,y_t) and (x_b,y_b) are located by firstly searching the boundary y-coordinates from the blob. The x-coordinates of the contact points can then be computed using Equation (1). Next, the top and bottom contact angles are computed from the circle parameters and the contact point coordinates. Contact angles at the top and bottom surfaces can be estimated from a triangle defined by the contact point, the circle radius and the Euclidean distance between the circle origin and the channel edge. This principle is presented in Fig. 7.

Angles, α_1 and α_2, which are equivalent to the contact angle subtracted by 90 degrees can be determined as follows

$$\alpha_1 = \arcsin\left(\frac{y_0 - y_t}{r}\right) \tag{4}$$

$$\alpha_2 = \arcsin\left(\frac{y_b - y_0}{r}\right). \tag{5}$$

The contact is hydrophobic if $x_0 - x_b > 0$ and hydrophilic if $x_0 - x_b < 0$, in case where direction of the liquid flow is from left to right. The top and bottom contact angles in hydrophobic contact are:

$$\theta_t = \alpha_1 + 90° = \arcsin\left(\frac{y_0 - y_t}{r}\right) + 90° \tag{6}$$

$$\theta_b = \alpha_2 + 90° = \arcsin\left(\frac{y_b - y_0}{r}\right) + 90°. \tag{7}$$

The top and bottom contact angles in hydrophilic contact are:

$$\theta_t = 90° - \alpha_1 = 90° - \arcsin\left(\frac{y_0 - y_t}{r}\right) \tag{8}$$

$$\theta_b = 90° - \alpha_2 = 90° - \arcsin\left(\frac{y_b - y_0}{r}\right). \tag{9}$$

3.3 Contact Angle Computation using Half Parabola Fittings:

Fitting a parabola to the coordinates of a liquid plug meniscus is performed similarly to the circle fitting. Using the meniscus coordinates, the equation of the parabola is determined by the least-squares method. Once the parabola is determined, slopes of tangents in the top and bottom contact points are determined. Based on the slopes, the top and bottom dynamic contact angles can be computed.

In the case when the meniscus shape is not uniform, using one circle or parabola might not be sufficient in the determination of the dynamic contact angle. For example, a defect on one channel wall might drastically change the contact angle on that wall. One possibility to enhance the accuracy in this case is to split the meniscus coordinates to two halves and make individual fittings. This was experimented by fitting two parabolas separately to the top and bottom halves of the meniscus coordinates. The parabola equations, for the top and bottom halves of the meniscus can be written as follows

$$x = f_{pt}(y) = a_{pt}y^2 + b_{pt}y + c_{pt} \tag{10}$$

$$x = f_{pb}(y) = a_{pb}y^2 + b_{pb}y + c_{pb} \tag{11}$$

where a_{pt}, b_{pt} and c_{pt} are the constants of a parabola equation of the top half and a_{pb}, b_{pb} and c_{pb} are the constants of a parabola equation of the bottom half. The constants are determined using the least-squares method.

An example of determining the contact angles of a front meniscus of a liquid plug using parabola fittings is presented in Fig. 8. Parabola fittings are determined from the detected coordinates of the front meniscus. After this, the slopes of the parabola tangents in the top and bottom contact points (x_t, y_t) and (x_b, y_b) are determined as follows

$$k_{pt} = 2a_{pt}y_t + b_{pt} \tag{12}$$

$$k_{pb} = 2a_{pb}y_b + b_{pb}, \tag{13}$$

where k_{pt} and k_{pb} are the slopes of the tangents at the top and the bottom contact points, respectively.

The contact is hydrophobic if $k_{pt} > 0$ and $k_{pb} > 0$ and hydrophilic if $k_{pt} < 0$ and $k_{pb} < 0$, in case where direction of the liquid flow is from left to right. The dynamic contact angles for the top and bottom contact point of the front meniscus by half parabola fittings are as follows

$$\theta_t = \arctan\left(k_{pt}\right) + 90° = \arctan\left(2a_{pt}y_t + b_{pt}\right) + 90° \tag{14}$$

$$\theta_b = \arctan\left(k_{pb}\right) + 90° = \arctan\left(2a_{pb}y_b + b_{pb}\right) + 90° \tag{15}$$

where θ_t is a dynamic contact angle of the top contact line, θ_b is a dynamic contact angle of the bottom contact line.

4 EXPERIMENTAL VERIFICATION AND COMPARISON

The reliability of the algorithm is tested with laboratory measurements using the test setup described in Section 2.2. Materials used for the measurements are described in Subsection 4.1 and the measurement results and the estimation of their reliability are presented in Subsection 4.2. Subsection 4.3 demonstrates the measurement of the dynamic contact angles of the top and bottom contact points from both front and rear menisci.

4.1 Materials:

A small volume of DI water is driven into a microchannel (Section A in Channel CH1) using the syringe pump. The flow rate of 50 µl/min is used. The liquid flow is imaged at a frame rate of 7.5 Hz. The images are 8-bit grey scale images containing 768 x 1024 pixels. The circle and half parabola fittings are applied to five images picked from a set of 50 recorded images and they are compared to manual measurements of the contact angles.

The size of the syringe used in these tests is 1.0 ml and it is connected to the channel using plastic tubing and a pipette having a conic tip. Both, the tubing and the syringe, are filled with DI water. The channel is dried with compressed air after the test.

4.2 Error Estimation:

The dynamic contact angles of the front meniscus of liquid flow are determined using the algorithms described in Section 3. The contact angle values are computed using the two fitting methods and as a reference, measured manually with ImageJ software. Values obtained using the curve fittings are compared to the manually measured values and errors between them are computed. In Fig. 9, an example image with applied fittings and tangent lines is illustrated. Table 1 presents the computed and manually measured dynamic contact angles. In Table 2, the errors between the computed and the manual dynamic contact angles are given. With circle fitting, errors of dynamic contact angles of top and bottom contact points are 3.7 % and 5.3 % and with half parabola fittings, 3.4 % and 0.9 %.

Based on the images and the error computations, it is evident that the parabola fittings provide more accurate results than the circle fitting. Errors overall are not very large, except for the fifth image. In the image, it can be seen that the shape of the meniscus has become slightly triangular and therefore, the circle fitting does not apply very well. The fitting error is furthermore analyzed by computing the errors between the detected coordinates and the fitted coordinates. Error sums of the coordinates displacements are presented in Table 3. The sum of the errors in the circle fitting is divided by two, since it includes twice more points than the two parabola fittings method. According to the coordinate displacements, smaller sums of errors are clearly achieved with half parabola fittings.

The errors overall are slightly larger than previously presented [11]. This is due to the shapes of the menisci, which is not as uniform in this study (this is emphasized especially by the fifth image of the experiments).

In the experiment, a constant flow rate was used for creating the liquid plug flow. Therefore, the values of the dynamic contact angles should remain approximately constant. Instantaneous values of the dynamic contact angles were inspected from the image data using both fitting methods. Results are presented in Fig. 10. It can be seen that the dynamic contact angle value varies more with the circle fitting. Therefore, it can be concluded that the half parabola fittings provide more accurate results when the shape of the meniscus is not uniform or high flow rates are used.

4.3 Demonstration:

The determination of the dynamic contact angles of front and rear menisci is demonstrated in this subsection. The test setup described in Subsections 2.2 and 4.1 is used in this demonstration. A liquid plug flow is initiated by the syringe pump and a small volume of DI water is used. The liquid plug flow is imaged and the dynamic contact angles are determined using half parabola fittings method. An example image of the liquid plug flow is illustrated in Fig. 11. In Fig. 12, the determined dynamic contact angles in front and rear menisci are presented. Both, the top and bottom contact points are taken into consideration. The variation in the values of the dynamic contact angles is not significant. There is also a clear difference between the front and rear menisci values which also indicates successful measurements.

5 CONCLUSIONS AND FUTURE WORK

Machine vision based methods to measure the dynamic contact angle in microchannel flows was successfully developed and experimented as described in this article. Two methods, circle and half parabola fittings, were developed and compared. Generally, both fitting methods provide good results. Often the shapes of the menisci in liquid plug flows are not uniform. Therefore, using half parabola fittings is a more accurate method for the measurement as shown in this article. Half parabola fittings should provide also accurate measurement results with liquid flows of high flow rates, when the shape of the meniscus becomes more oval/parabolic.

The preliminary measurement results are very good. Errors are slightly larger than the values presented in ICNMM2008-62113 paper [11] due to the reason that a channel with relatively large channel defects was chosen for this study. Average errors for the dynamic contact angles of the top and bottom contact points are 4.5 % using circle fitting and 2.2 % using half parabola fittings.

The experimental measurements completed and described in this article were done off-line; the image data was recorded separately and afterwards applied to the algorithm. Simplification and rationalization of the measurement procedure enables a real-time implementation of the algorithm.

When considering this research from a microfluidic perspective, the channel structures used in the experiments were relatively large. However, implementation of a similar measurement system for a microscale channels should not be a problem. A digital camera and microscope optics should enable accurate measurements also in microscale channels.

The machine vision based measurements can be used also with liquids other than water. In microfluidic channels, such liquids as buffers, reagents and blood serums are typically used. Thanks to the vision based approach, the methods described in this work are also applicable with the above mentioned liquids. In the future, to experiment the developed measurement method with blood as test liquid is important. Experiments with blood in microchannels are common in developing point-of-care (POC) applications. Therefore, a study of blood properties in microchannel flows is justified and the developed measurement method can be useful in it.

ACKNOWLEDGMENTS

This research was done as a part of TEKES-funded PanFlow project and as a part of a project OPTIMI funded by the Academy of Finland (a grant number 117587) in Micro- and Nanosystems Research Group, Tampere University of Technology, Finland. We would like to thank Christian Dahmen from Microrobotics and Control Engineering group, University of Oldenburg, Germany for his experience and valuable guidance in digital image processing.

REFERENCES

[1] Nguyen, N-T., Wereley, S. T., "Fundamentals and Applications of Microfluidics", 1st ed., Artech House, Boston, 2002, 487 p.

[2] Li, L., Kang, K., Ye, D., "A Contact Angle Measurement Method for the Droplets in EWOD-based Chips", *Conference on Nano/Micro Engineered and Molecular Systems*, Bangkok, Thailand, 2007, pp. 1071-1075

[3] Sankowski, D., Strzecha, K., Jezewski, S., Senkara, J., Lobodzinski, W., "Computerized Device with CCD Camera for Measurement of Surface Tension and Wetting Angle in Solid-Liquid Systems", *Instrumentation and Measurement Technology Conference*, 1999, pp. 164-168

[4] Mohammadi, R., Finlay, W. H., Roa, W., Amirfazli, A., "Determination of Contact Angle of Microspheres by Microscopy Methods", *Proceedings of the International Conference on MEMS, NANO and Smart Systems*, 2003, pp. 84-88

[5] Zhang, J., Kwok, D. Y., "Lattice Boltzmann Simulations of Bubble Dynamics in Microchannels", *Proceedings of the 2004 International Conference on MEMS, NANO and Smart Systems*, 2004, pp. 78-83

[6] Homma, H., Chang-Ryong, L., Toshiyuki, K., Kunikazu, I., "Evaluation of Time Variation of Hydrophobicity of Silicone Rubber using Dynamic Contact Angle Measurement", *Proceedings of the 6th International Conference on Properties and Applications of Dielectric Materials*, 2000, pp. 637-640

[7] Cho, H., Kim, H-Y., Kang, J. Y., Kim, T. S., "How the Capillary Burst Microvalve Works", *Journal of Colloid and Interface Science 306*, 2007, pp. 379-385

[8] Shui, L., Eijkel, J. C. T., van den Berg, A., "Multiphase Flow in Micro- and Nanochannels", *Sensors and Actuators B 121*, 2007, pp. 263-276

[9] Adhesives Research, [25.1.2008], http://www.adhesivesresearch.com/,

[10] Gonzales, R. C., Woods, R. E., “Digital Image Processing”, 3rd ed., Prentice Hall, New Jersey, 2007, 954 p.

[11] Heiskanen, V., Marjanen K., Kallio P., ”Machine Vision based Measurement of Dynamic Contact Angle in Microchannel Flows, *6th International Conference on Nanochannels, Microchannels and Minichannels*, Darmstadt, Germany, 2008, 8 p.

FIGURES

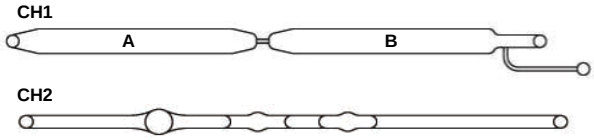

Figure 1. Flow channels.

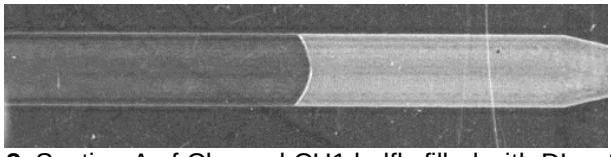

Figure 2. Section A of Channel CH1 halfly filled with DI water.

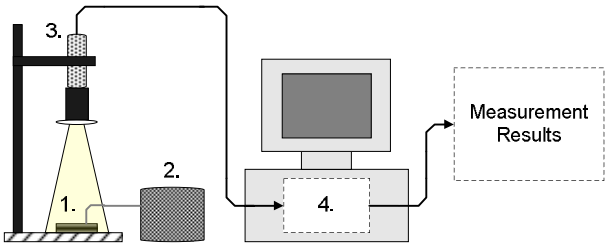

Figure 3. Machine vision based measurement setup; 1. Channel structure, 2. Flow control device, 3. Digital camera with optics, 4. Measurement computer with image processing algorithm.

a)

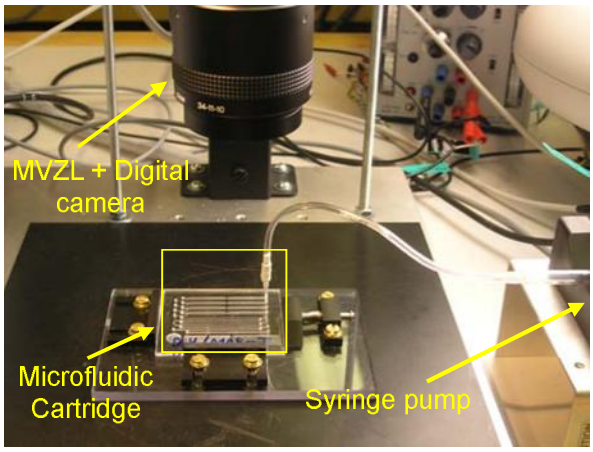

b)

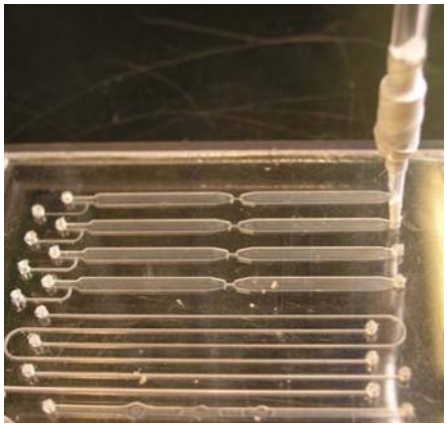

Figure 4. a) Photograph of measurement setup, b) Close-up of the channel structures.

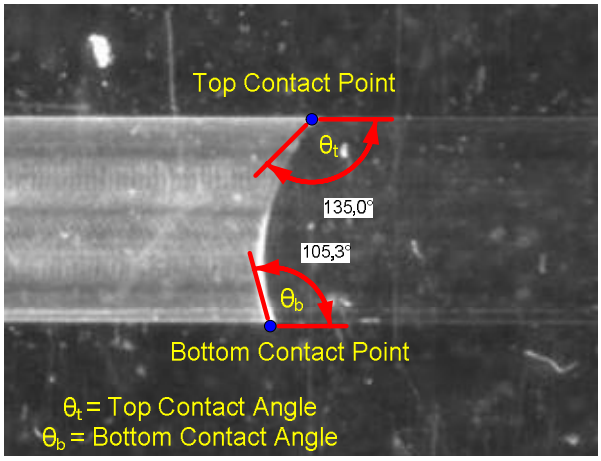

Figure 5. Dynamic contact angle determination from top and bottom borders of a channel.

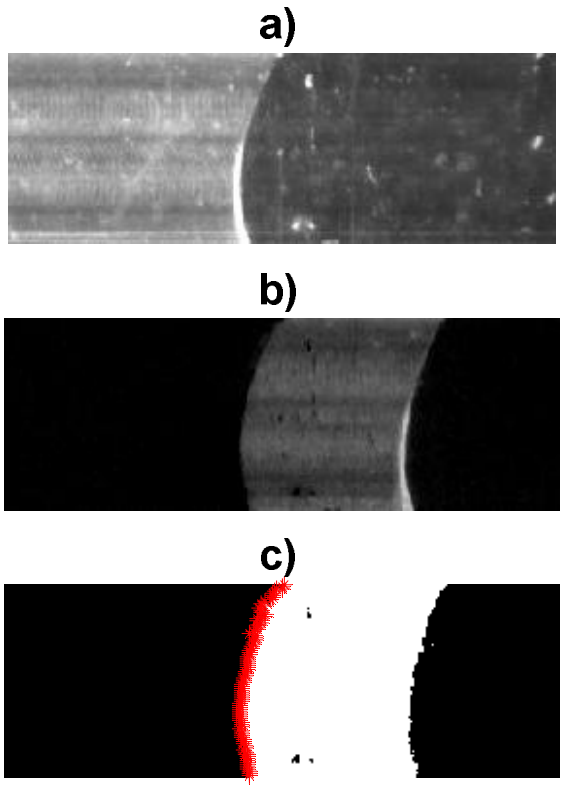

Figure 6. a) Liquid plug in an original image; b) Intensity frame, subtraction from previous frame; c) Thresholding and search of front meniscus coordinates.

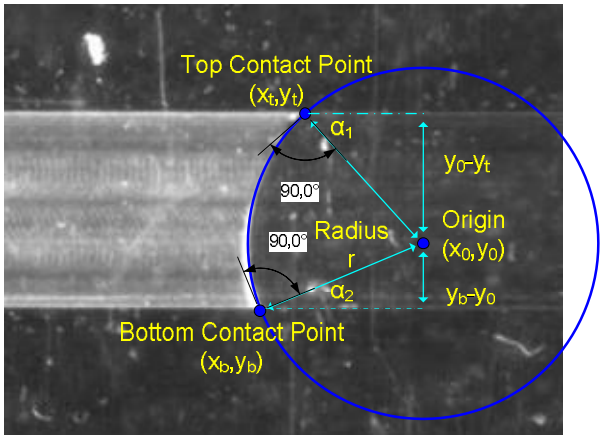

Figure 7. Dynamic contact angle by circle fitting.

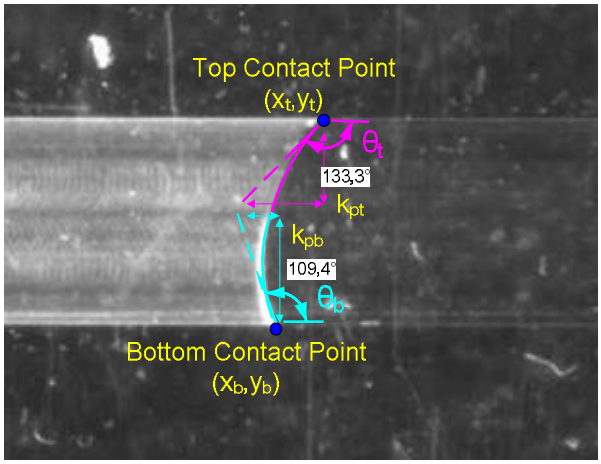

Figure 8. Dynamic contact angle by half parabola fittings.

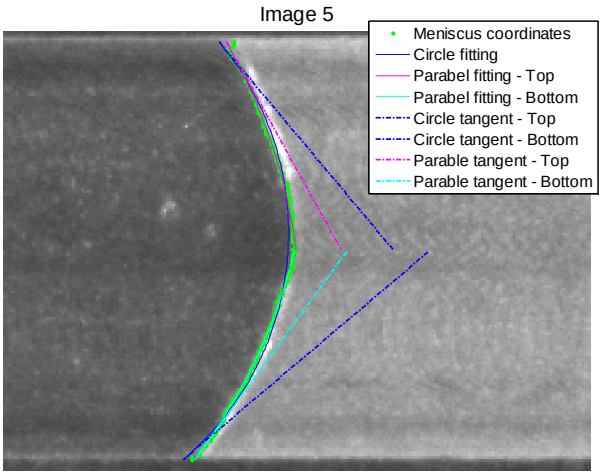

Figure 9. A front meniscus of a liquid plug with detected coordinates, applied fittings and tangents.

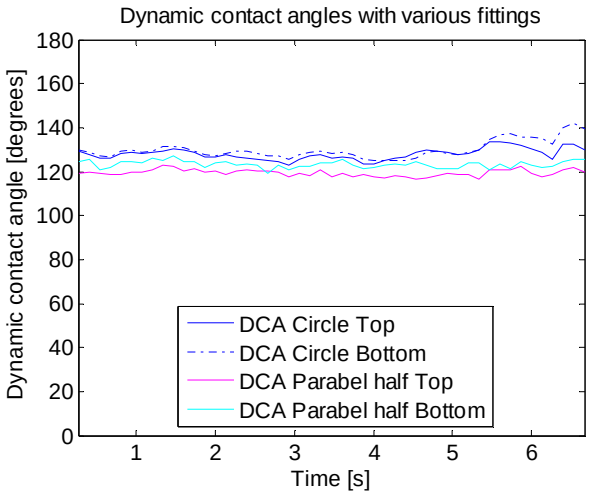

Figure 10. Instantaneous dynamic contact angles with both of the experimented fitting methods.

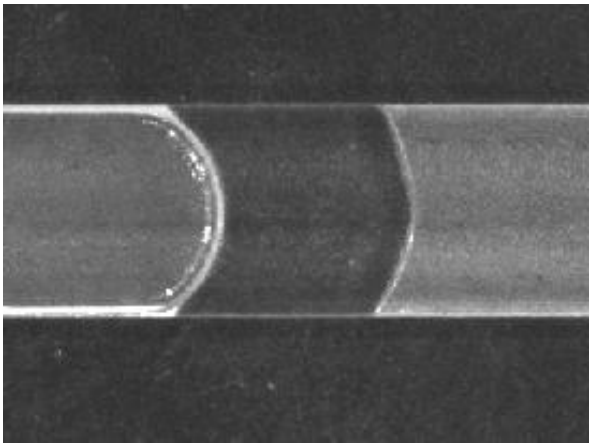

Figure 11. A single image illustrating liquid plug flow.

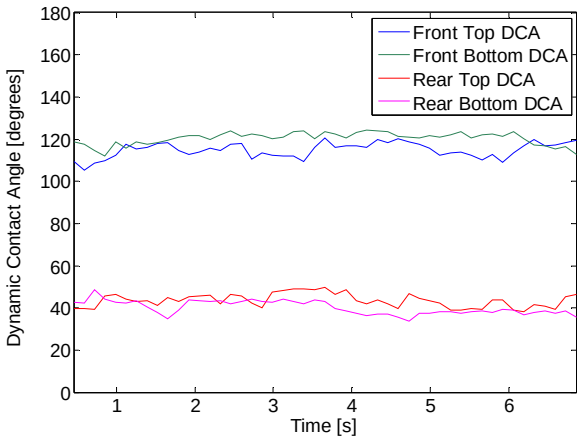

Figure 12. Instantaneous dynamic contact angles of front and rear menisci in liquid plug flow.

TABLES

Table 1. Measurement results for dynamic contact angles.

Measurement Methods of Dynamic Contact Angles						
Method	**Circle fitting (°)**		**Parabola half fittings (°)**		**Manual (°)**	
	Top	**Bottom**	**Top**	**Bottom**	**Top**	**Bottom**
1. Image	129.3	129.7	119.5	124.3	124.6	124.2
2. Image	130.2	131.5	122.1	126.9	124.7	125.0
3. Image	125.0	127.6	119.7	123.5	118.8	121.7
4. Image	124.9	125.3	117.1	123.0	122.0	121.3
5. Image	129.8	139.6	118.8	126.0	125.4	126.1

Table 2. Errors between fittings based and manual measurements.

Errors of Dynamic Contact Angles				
Errors compared to Manual	**Circle fitting Error (%)**		**Parabola half fittings Error (%)**	
	Top	**Bottom**	**Top**	**Bottom**
1. Image	3.6	4.2	4.3	0.1
2. Image	4.2	4.9	2.1	1.5
3. Image	5.0	4.6	0.8	1.5
4. Image	2.3	3.2	4.2	1.4
5. Image	3.4	9.7	5.6	0.1
Average	**3.7**	**5.3**	**3.4**	**0.9**

Table 3. Sums of errors of coordinate points.

Sums of errors between coordinate points and fitting points			
Fitting method	**Circle (pixels)**	**Parabola half (pixels)**	
		Top	**Bottom**
1. Image	70	32	36
2. Image	51	25	31
3. Image	38	27	34
4. Image	48	35	37
5. Image	104	35	29

LIST OF FIGURE CAPTIONS